LU TP 17-36

November 2017

Heavy charged scalars from $c\bar{s}$ fusion: A generic search strategy applied to a 3HDM with $\mathrm{U}(1) \times \mathrm{U}(1)$ family symmetry

José Eliel Camargo-Molina,[1,*] Tanumoy Mandal,[2,3,†]

Roman Pasechnik,[1,‡] and Jonas Wessén[1,§]

[1]*Department of Astronomy and Theoretical Physics, Lund University, SE-223 62 Lund, Sweden*

[2]*Department of Physics and Astronomy, Uppsala University, Box 516, SE-751 20 Uppsala, Sweden*

[3]*Department of Physics and Astrophysics, University of Delhi, Delhi 110007, India*

Abstract

We describe a class of three Higgs doublet models (3HDMs) with a softly broken $\mathrm{U}(1) \times \mathrm{U}(1)$ family symmetry that enforces a Cabibbo-like quark mixing while forbidding the tree-level flavour changing neutral currents. The hierarchy in the observed quark masses is partly explained by a softer hierarchy in the vacuum expectation values of the three Higgs doublets. As a consequence, the physical scalar spectrum contains a Standard Model (SM) like Higgs boson while exotic scalars couple the strongest to the second quark family, leading to rather unconventional discovery channels that could be probed at the Large Hadron Collider. In particular, we describe a search strategy for the lightest charged Higgs, through the process $c\bar{s} \to H^+ \to W^+ h_{125}$, using a multivariate analysis that leads to an excellent discriminatory power against the SM background. Although the analysis is applied to the proposed class of 3HDMs, we employ a model-independent formulation such that it can be applied to any other model with the same discovery channel.

* eliel@thep.lu.se

† tanumoy.mandal@physics.uu.se

‡ roman.pasechnik@thep.lu.se

§ jonas.wessen@thep.lu.se

I. INTRODUCTION

The Standard Model (SM) remarkably stands as one of the most successful theories in physics. However, it can still be considered rather *ad hoc* in its nature, with unexplained features that arise from fitting the experimental data. In addition, it fails to offer an explanation to several observed natural phenomena such as dark matter, neutrino masses, baryon asymmetry in the universe etc. It is then natural to study extensions of the SM that, while retaining its predictive power, offer explanations or shed light into the origin of e.g. the hierarchy of fermion masses or its rather specific flavor structure. There are a plethora of such beyond the SM (BSM) theories, but not many of those which offer unconventional features potentially testable by current measurements.

One of the simplest and most studied extensions are the so-called Two Higgs Doublet Models (2HDM) that add a second $\mathrm{SU(2)_L}$ doublet to the SM (an extensive review can be found in Ref. [1]). 2HDMs offer a plethora of interesting phenomenology and can lead to e.g. extra sources of CP violation, dark matter candidates and stable vacua at high energies. However, they typically introduce many new free parameters, fail to address the origin of the mass hierarchy in the fermion sector of the SM and require extra discrete symmetries to avoid tree-level Flavor Changing Neutral Currents (FCNCs).

Three Higgs Doublet Models (3HDM) have sparked interest in recent literature (see e.g. Refs. [2–7]). They retain most of the features of 2HDMs and could offer explanations to features of the SM, while leading to testable predictions at current collider experiments. With the increased field content, one can typically impose a higher symmetry leading to interesting flavour structures.

The most constraining abelian symmetry of the scalar potential in 3HDM's (see Eq. (3)) is $\mathrm{U(1)} \times \mathrm{U(1)}$ [8]. In this work, we promote the global $\mathrm{U(1)} \times \mathrm{U(1)}$ symmetry to the fermion sector (will be called $\mathrm{U(1)_X} \times \mathrm{U(1)_Z}$ in what follows) in such a way that (1) no tree-level FCNCs are present, (2) a Cabibbo-like mixing is enforced, and (3) the fermion mass hierarchies are related to a hierarchy in the three vacuum expectation values (VEVs) of the doublets. This leads to a model that, although being remarkably simple due to its high symmetry, is capable of both reproducing the current experimental data and yielding exotic collider signatures. The latter is due to the fact that, as a consequence of the model symmetries, the new scalar states (both charged and neutral) couple dominantly to the second quark family.

At the LHC, the searches of charged Higgs bosons are generally categorized into two mass regions depending on whether its mass $m_{H^\pm}$ is smaller or bigger than the top quark mass m_t. The motivation of this categorization comes from the properties of $H^\pm$ within the various 2HDM types or supersymmetric models. Usually, for a heavy charged Higgs ($m_{H^\pm} \gtrsim m_t$), the dominant production and decay channels in the LHC context are $pp \to H^- t\bar{b}\,[H^+\bar{t}b]$ and $H^+ \to t\bar{b}\ [H^- \to \bar{t}b]$, respectively [9, 10]. Apart from this channel, vector boson fusion ($W^\pm Z$ fusion) production of $H^\pm$ followed by the $H^\pm \to W^\pm Z$ decay is prominent in the Higgs triplet models such as Georgi-Machacek model [11]. This channel has also been searched for by ATLAS [12] and CMS [13] collaborations. A light charged Higgs ($m_{H^\pm} \lesssim m_t$) that decays to $\tau\bar{\nu}$ [10, 14], $c\bar{s}$ [15, 16] or $c\bar{b}$ [17] modes are also searched for at the LHC. Previously, at LEP, pair production of $H^\pm$ was considered where $H^\pm$ subsequently decays to a $W^\pm A$ pair [18, 19] (where A is a scalar with mass $m_A > 12$ GeV and predominantly decays to $b\bar{b}$ pairs).

Searches for heavy $H^\pm$ become increasingly important with the rise of the LHC center-of-mass energy and luminosity. Furthermore, it is also important to explore new production and decay modes of $H^\pm$ that are predicted by various BSM theories. In this paper, we particularly focus on a new search channel where $H^\pm$ resonantly decays to a $W^\pm h_{125}$ pair after being produced from $c\bar{s}$ ($\bar{c}s$) fusion. This rather uncommon search channel leads to testable predictions of our model at current LHC energies. In Refs. [20–22], the $H^\pm \to W^\pm h_{125}$ decay is considered where the H^- $[H^+]$ is produced in association with a $t\bar{b}$ $[\bar{t}b]$ pair. In our case, H^+ is produced singly in s-channel resonance through $c\bar{s}$ fusion. In Ref. [23], the possibility of sizable $c\bar{s} \to H^+$ production cross section is discussed in the SUSY context where a squark mixing can circumvent the chiral suppression of the single $H^\pm$ production. In our model, we will see that the chiral suppression of the $c\bar{s}H^+$ and $\bar{c}sH^-$ couplings are compensated by the presence of small VEVs in the denominators.

In section II, we introduce the model including the fermion and scalar sectors and their interplay as given by the $\mathrm{U(1)_X \times U(1)_Z}$ symmetry, the VEV hierarchy and the spectrum of the theory. In section III, we discuss the charged Higgs production and decay channels of the model and introduce a model-independent way to treat a theory with the same unconventional channels. In section IV, we show the results of a multivariate analysis for the charged Higgs searches and show, by using the results of a genetic algorithm scan, that our proposed theory can produce the type of signals visible with such an analysis at the LHC. Finally, we summarize and conclude our results in section VI.

II. THE MODEL

In this work, we propose a 3HDM, with two particular features that lead to a simple yet predictive model. The model has a $\mathrm{U}(1)_\mathrm{X} \times \mathrm{U}(1)_\mathrm{Z}$ global symmetry that maximally constrains its scalar potential. As a consequence, in the limit of one VEV being much larger than the other two, we can derive simple analytical formulas for masses and rotations in the scalar sector and readily understand the features of the model and its physical consequences.

The $\mathrm{U}(1)_\mathrm{X} \times \mathrm{U}(1)_\mathrm{Z}$ is also present in the fermion sector of the theory. We chose the charge assignments to constrain the Yukawa sector in a manner consistent with the experimental hierarchies in the quark mass spectrum and forbidding the tree-level FCNCs from the scalar sector. The upside of this is that the mass hierarchy is directly connected to a VEV hierarchy, which needs not to be as strong as the hierarchy in the SM Yukawa parameters to explain the known experimental results.

A nice consequence is the opening of new search strategies for testing this model at collider experiments, in particular, at the LHC. Due to the structure of the Yukawa sector, the two physical charged Higgs bosons would be produced mainly through $c\bar{s}$ fusion, which coupled with the appropriate techniques (as will be shown in section IV) can lead to good signal-to-background ratios. In the following, we will present in detail the different features of the model, focusing on its fermion and scalar sectors.

A. VEV hierarchy and the softly broken $\mathrm{U}(1)_\mathrm{X} \times \mathrm{U}(1)_\mathrm{Z}$ symmetry

Besides the field content of the SM, the model has two additional scalar $\mathrm{SU}(2)_\mathrm{L}$ doublets for a total of three. We will denote them by H_i, with charges as in table I, and expand around the vacuum as

$$H_i = \begin{pmatrix} H_i^+ \\ \frac{1}{\sqrt{2}}\left(v_i + h_i + \mathrm{i}A_i\right) \end{pmatrix} . \tag{1}$$

Often in this work, we will focus on the case where $v_3 \gg v_{1,2}$. This particular limit calls for the definition of a small parameter ξ,

$$\xi \equiv \frac{\sqrt{v_1^2+v_2^2}}{v_3}\,. \tag{2}$$

In the limit $\xi \to 0$, $\mathrm{U(1)_X}$ is unbroken, meaning that all $\mathrm{U(1)_X}$ violating processes would be suppressed by some power of ξ. As we will see, in the limit that $\xi \ll 1$ it is possible to derive simple expressions for the masses and mixing matrices in the scalar sector. It is worth noting at this stage that, while the expressions serve as tools to understand the model's features, all scalar masses and mixing matrices are computed fully numerically at arbitrary ξ when scanning the parameter space of the model.

A spontaneously broken $\mathrm{U(1)_X}\times\mathrm{U(1)_Z}$ global symmetry would lead to massless Goldstone bosons and constrain the model significantly when considering e.g. the precise measurements of the Z-boson width. This motivates us to softly break the symmetry by adding mass terms in the scalar potential. The scalar potential consistent with a softly broken $\mathrm{U(1)_X}\times\mathrm{U(1)_Z}$ global symmetry group can be split in fully symmetric and soft-breaking parts as $V = V_0 + V_{\text{soft}}$, where

$$V_0 = -\mu_i^2|H_i|^2 + \frac{\lambda_{ij}}{2}|H_i|^2|H_j|^2 + \frac{\lambda'_{ij}}{2}|H_i^\dagger H_j|^2\,, \quad V_{\text{soft}} = \frac{1}{2}m_{ij}^2(H_i^\dagger H_j + \text{c.c}) \tag{3}$$

with

$$\lambda_{ij} = \lambda_{ji}\,, \quad \lambda'_{ij} = \lambda'_{ji}\,, \quad m_{ij}^2 = m_{ji}^2\,, \tag{4}$$

$$\lambda'_{11} = \lambda'_{22} = \lambda'_{33} = 0\,, \quad m_{11}^2 = m_{22}^2 = m_{33}^2 = 0\,. \tag{5}$$

All parameters in the scalar potential can be taken real without any loss of generality. For convenience we define

$$\tilde{\lambda}_{ij} = (\lambda_{ij} + \lambda'_{ij})\,. \tag{6}$$

Assuming $v_{1,2,3} \neq 0$, the first derivatives of V vanish when

$$\mu_i^2 = \sum_j \left[\frac{1}{2}\tilde{\lambda}_{ij}v_j^2 + m_{ij}^2\frac{v_j}{v_i}\right]\,. \tag{7}$$

B. Extending the $\mathrm{U(1)_X}\times\mathrm{U(1)_Z}$ to the fermion sector

We assign the quark $\mathrm{U(1)_X}\times\mathrm{U(1)_Z}$ charges such that the neutral component of H_3 couples to only up- and down-type quarks of the third generation while the neutral components

	$\mathrm{U(1)_Y}$	$\mathrm{U(1)_X}$	$\mathrm{U(1)_Z}$
H_1	$\frac{1}{2}$	-1	$-\frac{2}{3}$
H_2	$\frac{1}{2}$	1	$\frac{1}{3}$
H_3	$\frac{1}{2}$	0	$\frac{1}{3}$
$Q_{\mathrm{L}}^{1,2}$	$\frac{1}{6}$	γ	δ
Q_{L}^{3}	$\frac{1}{6}$	β	α
$u_{\mathrm{R}}^{1,2}$	$\frac{2}{3}$	$1+\gamma$	$\frac{1}{3}+\delta$
t_{R}	$\frac{2}{3}$	β	$\frac{1}{3}+\alpha$
$d_{\mathrm{R}}^{1,2}$	$-\frac{1}{3}$	$1+\gamma$	$\frac{2}{3}+\delta$
b_{R}	$-\frac{1}{3}$	β	$-\frac{1}{3}+\alpha$

TABLE I. $\mathrm{U(1)_X}$, $\mathrm{U(1)_Z}$ and $\mathrm{U(1)_Y}$ (hypercharge) charges.

of H_1 and H_2 couple to the first and second generation down-type and up-type quarks, respectively, i.e.

$$\mathcal{L}^{\mathrm{q}}_{\mathrm{Yukawa}} = \sum_{i,j=1}^{2} \left\{ y^{\mathrm{d}}_{ij} \bar{d}^i_{\mathrm{R}} H_1^\dagger Q^j_{\mathrm{L}} - y^{\mathrm{u}}_{ij} \bar{u}^i_{\mathrm{R}} \tilde{H}_2^\dagger Q^j_{\mathrm{L}} \right\} + y_{\mathrm{b}} \bar{b}_{\mathrm{R}} H_3^\dagger Q^3_{\mathrm{L}} - y_{\mathrm{t}} \bar{t}_{\mathrm{R}} \tilde{H}_3^\dagger Q^3_{\mathrm{L}} + \text{c.c.}\,. \tag{8}$$

In this way, we enforce a Cabibbo-like quark mixing, where the gauge eigenstates of the third quark family are aligned with the corresponding flavour eigenstates. This also means that a hierarchy in the VEVs of the Higgs doublets, where $v_3 \gg v_{1,2}$, leads to a third quark family that is much heavier than the first two families without a strong hierarchy in the Yukawa couplings. In Table I, we show the most general quark charge assignments allowing the terms in Eq. (8) once the $\mathrm{U(1)_X} \times \mathrm{U(1)_Z}$ charges of $H_{1,2,3}$ are fixed. As long as the parameters α, β, γ and δ in Table I satisfy

$$(\beta-\gamma, \alpha-\delta) \notin \{(-1,-1),(-1,0),(0,0),(1,0),(1,1),(2,1)\}\,, \tag{9}$$

the terms in Eq. (8) are also the *only* allowed quark Yukawa interactions.

It is much more convenient to write the interactions of Eq. (8) in terms of physical parameters. In the mass basis, free parameters in the quark sector are simply the quark masses and the Cabibbo angle,

$$\begin{aligned} \mathcal{L}^{\mathrm{q}}_{\mathrm{Yukawa}} = &- \frac{\sqrt{2} m_{\mathrm{u}}}{v_2} \bar{u}_{\mathrm{R}} \tilde{H}_2^\dagger q^1_{\mathrm{L}} - \frac{\sqrt{2} m_{\mathrm{c}}}{v_2} \bar{c}_{\mathrm{R}} \tilde{H}_2^\dagger q^2_{\mathrm{L}} - \frac{\sqrt{2} m_{\mathrm{t}}}{v_3} \bar{t}_{\mathrm{R}} \tilde{H}_3^\dagger q^3_{\mathrm{L}} \\ &+ \frac{\sqrt{2} m_{\mathrm{d}}}{v_1} \bar{d}_{\mathrm{R}} H_1^\dagger q^1_{\mathrm{L}} + \frac{\sqrt{2} m_{\mathrm{s}}}{v_1} \bar{s}_{\mathrm{R}} H_1^\dagger q^1_{\mathrm{L}} + \frac{\sqrt{2} m_{\mathrm{b}}}{v_3} \bar{b}_{\mathrm{R}} H_3^\dagger q^2_{\mathrm{L}}\,. \end{aligned} \tag{10}$$

The reader might note that at higher orders, the Yukawa interactions only allow for a mixing between the first and second quark generations, thus opening the question of how to reproduce the observed full CKM mixing in the quark sector. As this model is thought as an effective theory, one can write the following dimension-6 operators consistent with the incident symmetries

$$\begin{aligned} &\bar{d}_{\rm R}^{1,2}\left(H_i^\dagger Q_{\rm L}^3\right)\left(H_j^\dagger H_k\right)\,, \quad \bar{u}_{\rm R}^{1,2}\left(\tilde{H}_i^\dagger Q_{\rm L}^3\right)\left(H_j^\dagger H_k\right)\,, \\ &\bar{b}_{\rm R}\left(H_i^\dagger Q_{\rm L}^{1,2}\right)\left(H_j^\dagger H_k\right)\,, \quad \bar{t}_{\rm R}\left(\tilde{H}_i^\dagger Q_{\rm L}^{1,2}\right)\left(H_j^\dagger H_k\right)\,. \end{aligned} \tag{11}$$

Such terms will induce naturally small (suppressed by the scale of new physics) mixing terms with the third quark family once Higgs VEVs appear. The operators can in principle be generated à la Frogatt-Nielsen [24] by integrating out the heavy fields of a high-energy theory. A deeper analysis of this is beyond the scope of this paper.

Finally, we note that the lepton Yukawa sector can be made very SM-like by assigning the lepton $\mathrm{U(1)_X} \times \mathrm{U(1)_Z}$ charges such that they only couple to H_3. We will assume that this is the case throughout this work, and not discuss the implications on lepton phenomenology any further. However, we want to point out that there are also other interesting scenarios, e.g. where the leptons couple to $H_{1,2,3}$ such that the lepton mass hierarchies are related to $v_{1,2} \ll v_3$, that can be studied further.

C. The spectrum, mixing matrices and interactions of the scalar sector

After spontaneous symmetry breaking, the mass terms in the scalar potential V in Eq. (3) can be neatly written as

$$V \ni \frac{1}{2} A_i (M_{\rm P}^2)_{ij} A_j + \frac{1}{2} h_i (M_{\rm S}^2)_{ij} h_j + H_i^- (M_{\rm C}^2)_{ij} H_j^+\,, \tag{12}$$

with

$$\begin{aligned} (M_{\rm P}^2)_{ij} &= m_{ij}^2 - \delta_{ij} \sum_k m_{ik}^2 \frac{v_k}{v_i}\,, \\ (M_{\rm S}^2)_{ij} &= \tilde{\lambda}_{ij} v_i v_j + (M_{\rm P}^2)_{ij}\,, \\ (M_{\rm C}^2)_{ij} &= \lambda'_{ij} v_i v_j - \delta_{ij} \sum_k \lambda'_{ik} v_k^2 + (M_{\rm P}^2)_{ij}\,. \end{aligned} \tag{13}$$

We note that both $M_{\rm C,P}^2$ have an eigenvector $\propto v_i$ with a zero eigenvalue. The corresponding Goldstone states become the longitudinal polarization states of the massive electroweak gauge bosons.

The electrically neutral scalar, pseudo-scalar and charged scalar mass eigenstates,

$$\bar{h}_i = (h_\mathrm{a}, h_\mathrm{b}, h_{125})_i \,, \quad \bar{A}_i = (A_\mathrm{a}, A_\mathrm{b}, A_\mathrm{G})_i \,, \quad \bar{H}_i^\pm = (H_\mathrm{a}^\pm, H_\mathrm{b}^\pm, H_\mathrm{G}^\pm)_i \,, \tag{14}$$

are related to the interaction eigenstates as

$$h_i = \mathsf{S}_{ij}\bar{h}_j \,, \quad A_i = \mathsf{P}_{ij}\bar{A}_j \,, \quad H_i^\pm = \mathsf{C}_{ij}\bar{H}_j^\pm \,, \tag{15}$$

The states A_G and $H_\mathrm{G}^\pm$ in Eq. (14) denote the Goldstone bosons. Working in the $\xi \ll 1$ limit, the mixing matrices S, P and C are identical up to $\mathcal{O}(\xi)$ but differ at $\mathcal{O}(\xi^2)$. It is here convenient to define an angle $\beta \in [0, \frac{\pi}{2}]$ as

$$\tan\beta = \frac{v_2}{v_1} \,. \tag{16}$$

To the second order in ξ, we have

$$\mathsf{S} = \mathsf{T} + \xi^2\mathsf{S}' \,, \quad \mathsf{P} = \mathsf{T} + \xi^2\mathsf{P}' \,, \quad \mathsf{C} = \mathsf{T} + \xi^2\mathsf{C}' \tag{17}$$

with

$$\mathsf{T} = \begin{pmatrix} 1 & X\xi & c_\beta\xi \\ -X\xi & 1 & s_\beta\xi \\ -c_\beta\xi & -s_\beta\xi & 1 \end{pmatrix}, \quad X \equiv \frac{m_{12}^2 s_\beta c_\beta}{m_{13}^2 s_\beta - m_{23}^2 c_\beta} \,. \tag{18}$$

For the $\mathcal{O}(\xi^2)$ pieces, we have

$$\mathsf{P}' = \begin{pmatrix} -\frac{1}{2}(X^2+c_\beta^2) & -\frac{1}{2}(1-Y)s_\beta c_\beta & 0 \\ -\frac{1}{2}(1+Y)s_\beta c_\beta & -\frac{1}{2}(X^2+s_\beta^2) & 0 \\ Xs_\beta & -Xc_\beta & 0 \end{pmatrix}, \mathsf{C}' = \mathsf{P}' + \begin{pmatrix} 0 & Z_1 & 0 \\ -Z_1 & 0 & 0 \\ 0 & 0 & 0 \end{pmatrix}, \mathsf{S}' = \mathsf{P}' + \begin{pmatrix} 0 & 0 & Z_2 \\ 0 & 0 & Z_3 \\ -Z_2 & -Z_3 & 0 \end{pmatrix}, \tag{19}$$

where

$$\begin{aligned} Y &= \frac{(2m_{12}^4 + m_{23}^4)c_\beta^2 - (2m_{12}^4 + m_{13}^4)s_\beta^2}{(m_{13}^2 s_\beta - m_{23}^2 c_b^2)^2} \,, \quad & Z_1 &= \frac{(\lambda_{23}' - \lambda_{13}')s_\beta^2 c_\beta^2 m_{12}^2 v_3^2}{(m_{13}^2 s_\beta - m_{23}^2 c_\beta)^2} \,, \\ Z_2 &= (\tilde{\lambda}_{13} - \lambda_{33})c_\beta^2 \frac{v_3^2}{m_{13}^2} \,, \quad & Z_3 &= (\tilde{\lambda}_{23} - \lambda_{33})s_\beta^2 \frac{v_3^2}{m_{23}^2} \,. \end{aligned} \tag{20}$$

Here, $Z_{1,2,3}$ parametrize the leading order difference in the mixings, which will be important as this determines the off-diagonal scalar-scalar interactions with the electro-weak gauge bosons. We also note that as X, Y, Z_1, Z_2, Z_3 get larger, the expansion in ξ becomes less reliable.

The state h_{125} contains mostly h_3, meaning that it couples substantially to the third quark family. It also receives a mass on the order of $v_3 \sim v$,

$$m_{h_{125}}^2 = \lambda_{33}v_3^2 + \mathcal{O}(\xi^2) \,, \tag{21}$$

making this state our candidate for the observed SM Higgs-like 125 GeV state. The exotic scalars $h_{\rm a,b}$, $A_{\rm a,b}$ and $H^{\pm}_{\rm a,b}$ are all heavy as the leading order contribution to their masses are inversely proportional to ξ. To the leading order, $\{h_{\rm a}, A_{\rm a}, H^{\pm}_{\rm a}\}$ are degenerate in mass. This is also the case for $\{h_{\rm b}, A_{\rm b}, H^{\pm}_{\rm b}\}$. More accurately, the masses are given by

$$\begin{aligned} m^2_{A_{\rm a}} = m^2_{h_{\rm a}} &= -\frac{m^2_{13}}{c_\beta \xi} - m^2_{12} t_\beta - (m^2_{13} c_\beta + X m^2_{12})\xi\,, \quad m^2_{H^\pm_{\rm a}} = m^2_{A_{\rm a}} - \lambda'_{13} v_3^2\,, \\ m^2_{A_{\rm b}} = m^2_{h_{\rm b}} &= -\frac{m^2_{23}}{s_\beta \xi} - \frac{m^2_{12}}{t_\beta} - (m^2_{23} s_\beta + X m^2_{12})\xi\,, \quad m^2_{H^\pm_{\rm b}} = m^2_{A_{\rm b}} - \lambda'_{23} v_3^2\,, \end{aligned} \tag{22}$$

to $\mathcal{O}(\xi)$.

We conclude this section by listing the trilinear interactions between the physical scalars and the electro-weak gauge bosons, as they are relevant for the collider phenomenology discussed in section III. The interactions between the neutral and charged scalars and the W boson are given by

$$\begin{aligned} \mathcal{L} &\supset {\rm i}\frac{g_2}{2}\left[(\partial^\mu H^+_i) h_i - H^+_i(\partial^\mu h_i)\right] W^-_\mu + {\rm c.c} \\ &= {\rm i}\frac{g_2}{2}(\mathsf{C}^{\rm T}\mathsf{S})_{ij}\left[(\partial^\mu \bar{H}^+_i)\bar{h}_j - \bar{H}^+_i(\partial^\mu \bar{h}_j)\right] W^-_\mu + {\rm c.c}\,, \end{aligned} \tag{23}$$

with

$$\mathsf{C}^{\rm T}\mathsf{S} = \begin{pmatrix} 1 & -Z_1\xi^2 & Z_2\xi^2 \\ Z_1\xi^2 & 1 & Z_3\xi^2 \\ -Z_2\xi^2 & -Z_3\xi^2 & 1 \end{pmatrix} + \mathcal{O}(\xi^3)\,. \tag{24}$$

The W boson similarly couples to pairs of charged scalars and pseudo-scalars as

$$\begin{aligned} \mathcal{L} &\supset \frac{g_2}{2}\left[(\partial^\mu H^+_i) A_i - H^+_i(\partial^\mu A_i)\right] W^-_\mu + {\rm c.c} \\ &= \frac{g_2}{2}(\mathsf{C}^{\rm T}\mathsf{P})_{ij}\left[(\partial^\mu \bar{H}^+_i)\bar{A}_j - \bar{H}^+_i(\partial^\mu \bar{A}_j)\right] W^-_\mu + {\rm c.c}\,, \end{aligned} \tag{25}$$

with

$$\mathsf{C}^{\rm T}\mathsf{P} = \begin{pmatrix} 1 & -Z_1\xi^2 & 0 \\ Z_1\xi^2 & 1 & 0 \\ 0 & 0 & 1 \end{pmatrix} + \mathcal{O}(\xi^3)\,. \tag{26}$$

Similarly, for the trilinear interactions with the Z boson, we have

$$\begin{aligned} \mathcal{L} &\supset \frac{g_2}{2c_{\rm W}}\left[(\partial^\mu A_i) h_i - A_i(\partial^\mu h_i)\right] Z_\mu \\ &= \frac{g_2}{2}(\mathsf{P}^{\rm T}\mathsf{S})_{ij}\left[(\partial^\mu \bar{A}_i)\bar{h}_j - \bar{A}_i(\partial^\mu \bar{h}_j)\right] Z_\mu, \end{aligned} \tag{27}$$

with

$$\mathsf{P}^{\rm T}\mathsf{S} = \begin{pmatrix} 1 & 0 & Z_2\xi^2 \\ 0 & 1 & Z_3\xi^2 \\ -Z_2\xi^2 & -Z_3\xi^2 & 1 \end{pmatrix} + \mathcal{O}(\xi^3)\,. \tag{28}$$

D. Scalar-fermion couplings

When knowing the mixing matrices S, P and C for the neutral scalars, pseudo-scalars and charged scalars to the first orders in ξ, it is straightforward to obtain the Yukawa interactions between the physical scalars and the quarks by plugging Eqs. (15) into Eq. (10). Doing so, we find that h_{125} couples to the quarks as

$$\mathcal{L} \supset \sum_q \frac{m_q}{v_3} \bar{q} q h_{125} + \mathcal{O}(\xi)\,, \tag{29}$$

i.e. with an interaction strength that is slightly enhanced (by a factor v/v_3) with respect to the corresponding coupling in the SM. For the third quark family, this is an obvious consequence of the model's symmetries, as t and b quarks receive their masses from H_3 with $v_3 \lesssim v$, and h_{125} is mostly made of h_3. The first and second family on the other hand get their masses from $H_{1,2}$ with $v_{1,2} \ll v_3$ so the corresponding Yukawa couplings with $H_{1,2}$ are quite large, $\mathcal{O}(m_q/v_{1,2}) \sim \mathcal{O}(m_q/\xi v_3)$. However, $h_{1,2}$ contains an $\mathcal{O}(\xi)$ amount of h_{125} so the couplings to h_{125} become $\mathcal{O}(m_q/v_3)$.

In the same process we also find the interaction terms between the quarks and the exotic scalar states $h_{\rm a,b}$, $A_{\rm a,b}$ and $H^\pm_{\rm a,b}$. Couplings to the third quark family are generally quite small, $\sim \frac{m_{\rm t,b}}{v_3}\xi$. Rather, the phenomenologically most relevant couplings are instead with the second quark family, which to the leading order in ξ reads

$$\begin{aligned} \mathcal{L} \supset & \frac{\sqrt{2} m_{\rm s}}{v_1} \bar{s}_{\rm R} c_{\rm L} H^-_{\rm a} - \frac{\sqrt{2} m_{\rm c}}{v_2} \bar{c}_{\rm R} s_{\rm L} H^+_{\rm b} + \text{c.c.} \\ & + \frac{m_{\rm s}}{v_1} \bar{s} s h_{\rm a} - \frac{m_{\rm c}}{v_2} \bar{c} c h_{\rm b} + {\rm i} \frac{m_{\rm s}}{v_1} \bar{s} \gamma^5 s A_{\rm a} - {\rm i} \frac{m_{\rm c}}{v_2} \bar{c} \gamma^5 c A_{\rm b}\,. \end{aligned} \tag{30}$$

When the masses of the scalars are in the appropriate range, we therefore expect that the charged scalars $H^+_{\rm a,b}$ would be produced in collider experiments through $c\bar{s}$ fusion while $h_{\rm a}$ and $A_{\rm a}$ ($h_{\rm b}$ and $A_{\rm b}$) would mainly be produced by fusing $s\bar{s}$ ($c\bar{c}$) pairs.

III. A MODEL INDEPENDENT APPROACH

One of the interesting features of our model is the existence of heavy charged scalars H^+ (H^-) that mostly couple to a $c\bar{s}$ ($\bar{c}s$) pair as their interactions with $t\bar{b}$ ($\bar{t}b$) are small due to the model symmetries. Furthermore, we find that $H^\pm$ can decay to a $W^\pm h_{125}$ pair with a sizable branching ratio (BR) which is still allowed by the current experimental data. It turns out that this unconventional channel, while not explored in the literature before, can be a rather clean way to search for charged scalars at the LHC.

In the following, we adopt a model independent approach to the search for charged scalars exhibiting those features. In section V, we will show how the analysis can be used to find discovery regions in the parameter space of the 3HDM we have proposed above. We take a model independent approach to not only test the predictions of our model but also offer a guideline for our experimental colleagues to implement this new search channel.

We start with the following model independent Lagrangian for $H^\pm$ including its kinetic ($\mathcal{L}_{kin}$) and interaction ($\mathcal{L}_{int}$) terms

$$\mathcal{L}_{kin} \supset D_\mu H^+ D^\mu H^- - m_{H^\pm}^2 \; H^+ H^- \,, \tag{31}$$

$$\mathcal{L}_{int} \supset \kappa_{cs}^p \; \bar{c}_{\rm R} s_{\rm L} H^+ + \kappa_{cs}^m \; \bar{s}_{\rm R} c_{\rm L} H^- + i\kappa_{Wh_{125}} \; \left(h_{125}\partial^\mu H^+ - H^+ \partial^\mu h_{125}\right) W_\mu^- + \text{c.c.}\,. \tag{32}$$

There are four free parameters in the above Lagrangian *viz.* the charged Higgs mass $m_{H^\pm}$, and the three couplings κ_{cs}^p, κ_{cs}^m and $\kappa_{Wh_{125}}$. In general, κ_{cs}^p and κ_{cs}^m both could be nonzero. In that case, the production cross section, $\sigma(pp \to H^\pm)$ is proportional to the combination $\left[(\kappa_{cs}^p)^2 + (\kappa_{cs}^m)^2\right]$. Therefore, instead of two free couplings, we introduce a single free parameter κ_{cs} which is, $\kappa_{cs}^2 = (\kappa_{cs}^p)^2 + (\kappa_{cs}^m)^2$. From the above model independent Lagrangian, H^+ has only two decay modes $W^+ h_{125}$ and $c\bar{s}$ and the corresponding partial widths are given by

$$\begin{aligned}
\Gamma\left(H^\pm \to W^\pm h_{125}\right) &= \frac{\kappa_{Wh_{125}}^2 m_{H^\pm}^3}{64\pi m_W^2}\left[1 - \frac{\left(m_{h_{125}} - m_W\right)^2}{m_{H^\pm}^2}\right]\left[1 - \frac{\left(m_{h_{125}} + m_W\right)^2}{m_{H^\pm}^2}\right] \\
&\times \left[1 - \frac{2\left(m_{h_{125}}^2 + m_W^2\right)}{m_{H^\pm}^2} + \frac{\left(m_{h_{125}}^2 - m_W^2\right)^2}{m_{H^\pm}^4}\right]^{1/2} , \qquad (33)\\
\Gamma\left(H^+ \to c\bar{s}\right) &= \frac{3\left[(\kappa_{cs}^p)^2 + (\kappa_{cs}^m)^2\right] m_{H^\pm}}{16\pi} = \frac{3\kappa_{cs}^2 m_{H^\pm}}{16\pi}\,. \qquad (34)
\end{aligned}$$

where $m_{h_{125}} = 125$ GeV. The expression $\Gamma(H^+ \to c\bar{s})$ is given in the limit of massless c and s quarks. In general, $H^\pm$ can have other decay modes too. We, therefore, take the BR of the decay mode $H^\pm \to W^\pm h_{125}$ denoted by $\text{BR}_{Wh_{125}}$ as a free parameter instead of $\kappa_{Wh_{125}}$. So, one can write the following in the narrow width approximation,

$$\sigma(pp \to H^\pm \to W^\pm h_{125}) = \sigma(pp \to H^\pm) \times \text{BR}_{Wh_{125}} = \kappa_{cs}^2 \times \sigma_0(m_{H^\pm}) \times \text{BR}_{Wh_{125}}\,, \tag{35}$$

where $\sigma_0(m_{H^\pm})$ is the cross section of $pp \to H^\pm$ for $\kappa_{cs} = 1$. We show $\sigma_0(m_{H^\pm})$ at the LHC ($\sqrt{s} = 13$ TeV) as a function of $m_{H^\pm}$ in Fig. 1.

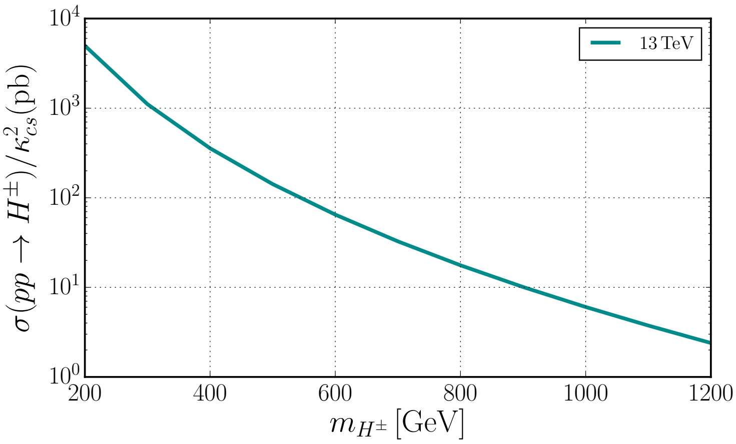

FIG. 1. $\sigma(pp \to H^{\pm})$ as a function of $m_{H^\pm}$ at the LHC ($\sqrt{s}$ = 13 TeV). We show the cross section by dividing κ_{cs}^2 that is basically $\sigma_0(m_{H^\pm})$ as defined in the text.

IV. SEARCH FOR CHARGED SCALARS PRODUCED BY $c\bar{s}$ FUSION

We implement the model independent Lagrangian of $H^\pm$ as shown in Eqs. (31) and (32) in FeynRules [25] from which we get the Universal FeynRules Output [26] model files for the MadGraph [27] event generator. We use the NNPDF [28] parton distribution functions (PDFs) for the signal and background event generation. For the signal, we use a fixed factorization μ_F and renormalization μ_R scales at $\mu_F = \mu_R = m_{H^\pm}$ while for the background these scales are chosen at the appropriate scale of the process. We use Pythia6 [29] for subsequent showering and hadronization of the generated events. Detector simulation is performed using Delphes [30] which employs the FastJet [31] package for jet clustering. Jets are clustered using the anti-kT algorithm [32] with the clustering parameter $R = 0.4$. For the multivariate analysis (MVA), we use the Boosted Decision Tree (BDT) algorithm in the TMVA [33] framework. In this analysis, all calculations are done at the leading order, for simplicity.

A. Signal

We focus the H^+ (H^-) production from the $c\bar{s}$ ($\bar{c}s$) initial state followed by the decay $H^\pm \to W^\pm h_{125}$. We consider a semileptonic final state where $W^\pm$ decays leptonically and h_{125} decays to $b\bar{b}$. Therefore, the chain of the signal process in our case is

$$pp \to H^{\pm} \to W^{\pm} h_{125} \to \ell^{\pm} + \not{E}_T + b\bar{b} \ . \tag{36}$$

Here, $\ell = \{e, \mu\}$. So, we have one charged lepton, two b-jets and missing transverse energy in the final state and our event selection criteria is exactly one charged lepton (either an electron or a muon including their antiparticles), at least, two jets and missing transverse energy that pass the following basic selection cuts:

- Lepton: $p_T(\ell) > 25$ GeV, $|\eta(\ell)| < 2.5$
- Jet: $p_T(J) > 25$ GeV, $|\eta(J)| < 4.5$
- Missing transverse energy: $\not{E}_T > 25$ GeV
- ΔR separation: $\Delta R(J_1, J_2) > 0.4$, $\Delta R(\ell, J) > 0.4$

Here, J_1 and J_2 denote the first and the second highest p_T jets. After selecting the events, we further demand b-tagging on the two leading-p_T jets. The b-tagging on jets can reduce the background very effectively but it can also reduce the signal somewhat. To enhance the signal cut efficiency we, therefore, not always demand two b's tagging although there are two b-jets present in the signal. Depending on the number of b-tagged jets one demands, we define the following two signal categories

- 1b-tag: In this category, we demand at least one b-tagged jet among the two leading p_T jets.
- 2b-tag: In this category, we demand that both the two leading p_T jets are b-tagged. This category is a subset of the 1b-tag category.

To reconstruct the Higgs boson, we apply an invariant mass cut $|m_{H^{\pm}} - m_{h_{125}}| < 20$ GeV around the Higgs boson mass $m_{h_{125}} = 125$ GeV. However, the full event is not totally recostructable due to the presence of the missing transverse energy.

B. Background

The main backgrounds for the signal with one lepton, at least, one or two b-tagged jets and missing energy can come from the following SM processes:

1. $W^{\pm}$ + jets: The definition of our inclusive $W^{\pm}$ + jets background includes up to two jets and we include the b parton in the jet definition i.e. $j = \{g, u, d, c, s, b\}$. We generate these background events in two separate parts. In one sample, we

Process	$W + n\ j$	Wbj	$Wb\bar{b}$	$t\bar{t} + n\ j$	tj	tb	tW	WW	WZ	Wh_{125}
x-sec (pb)	1.53×10^5	308.9	41.7	431.3	174.6	2.6	54.0	67.8	25.4	1.1

TABLE II. Parton-level cross sections of various backgrounds (without any cut) at the LHC ($\sqrt{s} = 13$ TeV).

only consider light jets i.e. $j = \{g, u, d, c, s\}$ and combine $pp \to W^{\pm} + (0, 1, 2)\ j$ processes where we set the matching scale $Q_{cut} = 25$ GeV. This background is the largest (cross section is about 1.53×10^5 pb at the LHC, with $\sqrt{s} = 13$ TeV, without any cut) among all the dominant SM backgrounds we have considered. Although the bare cross section is large, it will reduce drastically after b-tagging due to a small mistagging (light jet is tagged as b-jet) rate. We find that its contribution in the $1b$-tag category is substantial but in the $2b$-tag category is very small. In the other sample, we consider at least one b parton in the final state where we combine $pp \to W^{\pm} bj$ and $pp \to W^{\pm} b\bar{b}$ processes (no SM $pp \to W^{\pm} b$ process exists). This background will contribute significantly in both the categories. We include $pp \to W^{\pm} h_{125} \to W^{\pm} b\bar{b}$ and $pp \to W^{\pm} Z \to W^{\pm} b\bar{b}$ processes in the $pp \to W^{\pm} b\bar{b}$ channel.

2. $t\bar{t}$ + jets: The definition of our inclusive $t\bar{t}$ + jets background includes up to two jets containing also b partons. We generate this background by combining $pp \to t\bar{t} + (0, 1, 2)\ j$ processes using the matching scale $Q_{cut} = 25$ GeV. The matched cross section is about 431 pb before the top decay and without any selection cut applied. We find that this background is the dominant one after the strong basic selection cuts (applied before passing the events to the MVA).
3. Single top: This background includes three types of single top processes – s-channel single top (such $pp \to t\bar{b}$), t-channel single top (i.e. $pp \to tj$) and single-top associated with W (such as $pp \to tW^{\pm}$) processes. Note that for the $pp \to tW^{\pm}$ process, the selected lepton can come from two possible ways, either from the decay of the associated $W^{\pm}$ or from the $W^{\pm}$ coming from the top decay. These two possibilities are properly included in our event sample. The single top background also contributes significantly to the total background.
4. Diboson: This background includes $pp \to W^{\pm} W^{\mp} \to W^{\pm} + jj$ and $pp \to W^{\pm} Z \to W^{\pm} + jj$ processes where two light jets come from the decay of W or Z bosons. In

this background, we have also included $pp \to W^\pm Z \to W^\pm \nu\bar{\nu}$ processes where two selected jets come from the parton showers. This background reduces drastically due to the small mistagging efficiency of light jets that are misidentified as b-jets. Finally, in the MVA this background contributes negligibly to the total background. Note that two diboson production processes viz. $pp \to W^\pm h_{125} \to W^\pm b\bar{b}$ and $pp \to W^\pm Z \to W^\pm b\bar{b}$ processes are already considered in the $W+$jets background.

5. QCD multijets: The multijet background arises due to QCD interactions at the LHC and has a very large production cross section, especially in the soft region. The QCD-induced multijet production processes can potentially contribute to the total background for our signal by faking the lepton, $\not{E}_T$ and b-tagged jets. It is impractical to study this part of the background using a Monte-Carlo simulation since it is computationally challenging to generate enough events due to very low fake rates. In experimental analyses, this contribution is usually estimated from the data. In our analysis, we do not consider this background since it will be largely diminished after strong preselection cuts and will be further reduced due to small fake rates of the considered final states.

The SM background, especially the $W+$jets component is large, and therefore one has to design a clever set of cuts which would notably reduce such a background but not affect the signal much. This implies that the cut efficiency for the background is very small and hence, a large number of background events has to be generated. In order to avoid the generation of a large event sample, we apply a strong cut on the partonic center-of-mass energy, $\sqrt{\hat{s}} > 200$ GeV at the generation level of all backgrounds. This cut can reduce the $W+$jets background by two orders of magnitude. However, this cut has no or very little effect on the other backgrounds viz. $t\bar{t}+$jets, single top and diboson ones since the threshold energy for them is either above or slightly below 200 GeV. In the case of a signal, $\sqrt{\hat{s}}$ is always above 200 GeV since we are interested in the parameter space regions where $m_{H^\pm} > m_W + m_H \gtrsim 205$ GeV.

One should note that in reality the full reconstruction of $\sqrt{\hat{s}}$ of an event is not possible if there is a missing energy present in that event. In this case, one can construct an inclusive global variable $\sqrt{\hat{s}_{min}}$ defined in Ref. [34] which is closest to the actual $\sqrt{\hat{s}}$ of the event. One can roughly approximate $\sqrt{\hat{s}} \approx \sqrt{\hat{s}_{min}}$ if there is only one missing neutrino in the event but this approximation gets poorer with the increase of the number of neutrinos in the final state. For simplicity, we have used the cut $\sqrt{\hat{s}} > 200$ GeV at the generation level. But in reality, one can use a cut on $\sqrt{\hat{s}_{min}}$ to trim the background before passing it for further analysis.

C. Multivariate analysis

A Wh_{125} resonance, similar to our case, can also appear from the decay of a heavy charged gauge boson, W'. The search for W' in the $\ell^{\pm} + \not{E}_T + b\bar{b}$ channel (same final state that we are interested in) has been carried out at the LHC [35, 36]. In these searches, they mainly focus in the TeV-scale W' mass and the analyses are done using cut-based techniques. A cut-based analysis may not perform well in our case, especially for low $m_{H^{\pm}}$ region due to the presence of a large SM background [37, 38]. Therefore, we choose to use a MVA to obtain a better signal-to-background discrimination which usually leads to a better significance than a cut-based analysis. See Ref. [39] for a brief review on various multivariate methods and their use in collider searches. In this paper, we only use multivariate techniques and do not compare our achieved sensitivity with the cut-based techniques.

We choose the following twelve simple kinematic variables that are also listed in Table III for our MVA.

- Transverse momenta of lepton, $p_T(\ell)$ and two leading-p_T jets, $p_T(J_1)$ and $p_T(J_2)$.
- Missing transverse energy $\not{E}_T$ and pseudorapidity of $\not{E}_T$ vector denoted by $\eta(\not{E}_T)$.
- Scalar sum of transverse momenta of all visible particles denoted by H_T.
- Invariant mass of two leading-p_T jets denoted by $M(J_1, J_2)$.
- ΔR separation of (ℓ, J_1), (ℓ, J_2), $(\not{E}_T, \ell)$, (J_1, J_2) and $(\not{E}_T, J_1)$ combinations.

These variables are chosen by comparing their distributions for the signal generated for $m_{H^{\pm}} = 300$ GeV with the total background distributions. They are selected from a bigger set of variables based on their discriminating power and less correlation. In Fig. 2, we show the normalized distributions of these variables for the signal with $m_{H^{\pm}} = 300$ GeV and the total background. Similar distributions for $m_{H^{\pm}} = 500$ GeV are shown in Fig. 3. From these figures, one can see that each of these distributions has reasonable discriminating power between the signal and the background. We use these kinematic variables simultaneously in a MVA whose output shows large differences in their shapes for the signal and the background. One should notice that the signal distributions deviate more from the background ones as we increase $m_{H^\pm}$. Therefore, isolation of the signal from the background becomes easier for heavier resonances. We, therefore, tune our MVA for lower masses and use the same optimized analysis for larger masses.

Variable	Importance	Variable	Importance	Variable	Importance	Variable	Importance
$p_T(\ell)$	0.095	$\not{E}_T$	0.072	$M(j_1, j_2)$	0.092	$\Delta R(\not{E}_T, \ell)$	0.065
$p_T(j_1)$	0.092	$\eta(\not{E}_T)$	0.076	$\Delta R(\ell, j_1)$	0.088	$\Delta R(j_1, j_2)$	0.072
$p_T(j_2)$	0.074	H_T	0.153	$\Delta R(\ell, j_2)$	0.077	$\Delta R(\not{E}_T, j_1)$	0.044

TABLE III. Input variables used for MVA (BDT algorithm) and their relative importance. These numbers are obtained for $m_{H^\pm} = 300$ GeV for the $2b$-tag category. These numbers can vary for other choices of parameters.

In Table III, we show relative importance of each variable in the BDT response for $m_{H^\pm} = 300$ GeV for the $2b$-tag category. For this particular benchmark, the H_T variable has the highest relative importance of about 15%. The greater relative importance implies that the corresponding variable becomes a better discriminator. Note that the relative importance of such a variable can change for other benchmarks and for different LHC energies that can change the shape of the distributions. It can also change due to different choices of algorithms and their tuning parameters.

One should always be cautious while using the BDT algorithm since it is prone to overtraining. This can happen during the training of the signal and background test samples due to improper choices of the tuning parameters of the BDT algorithm. One can decide whether a test sample is overtrained or not by checking the corresponding Kolmogorov-Smirnov (KS) probability. If it lies within the range 0.1 to 0.9, we say the sample is not overtrained. We use two statistically independent samples in our MVA for each benchmark mass, one for training the BDT and another for testing purposes. In our analysis, we ensure that we do not encounter overtraning while using the BDT by checking the corresponding KS probablity.

In Figs. 4a and 4c, we display a normalized BDT output of the signal and the background for $m_{H^\pm} = 300$ GeV and $m_{H^\pm} = 500$ GeV, respectively, for the 2b-tag category at the LHC ($\sqrt{s} = 13$ TeV). One can see that the BDT outputs for the signal and the background

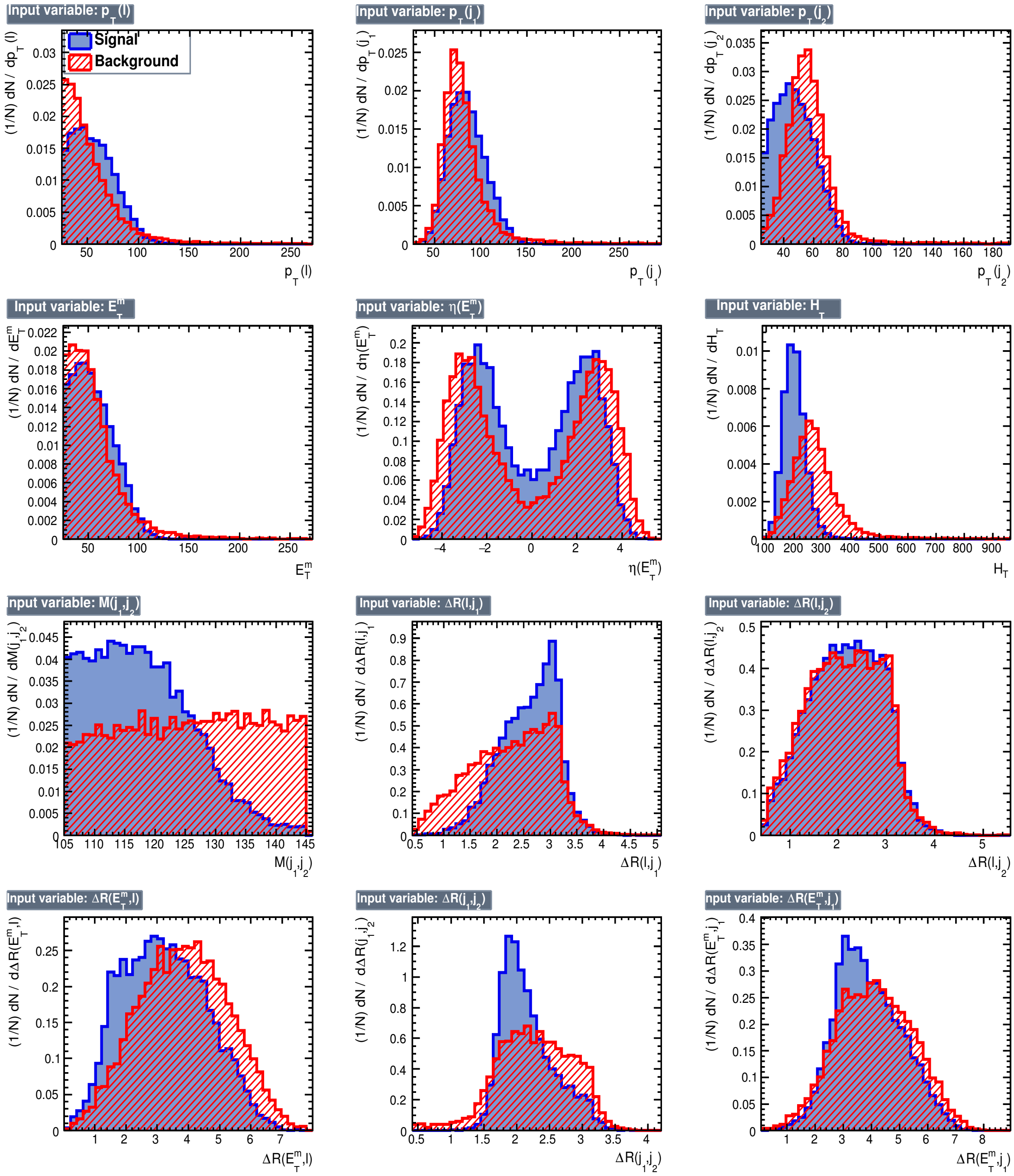

FIG. 2. Normalized distributions of the input variables at the LHC ($\sqrt{s}$ = 13 TeV) used in the MVA for the signal (blue) and the background (red). Signal distributions are obtained for $m_{H^\pm}$ = 300 GeV, and the background includes all the dominant backgrounds discussed in subsection IV B. These distributions are drawn by selecting events after the cuts defined in subsection IV A.

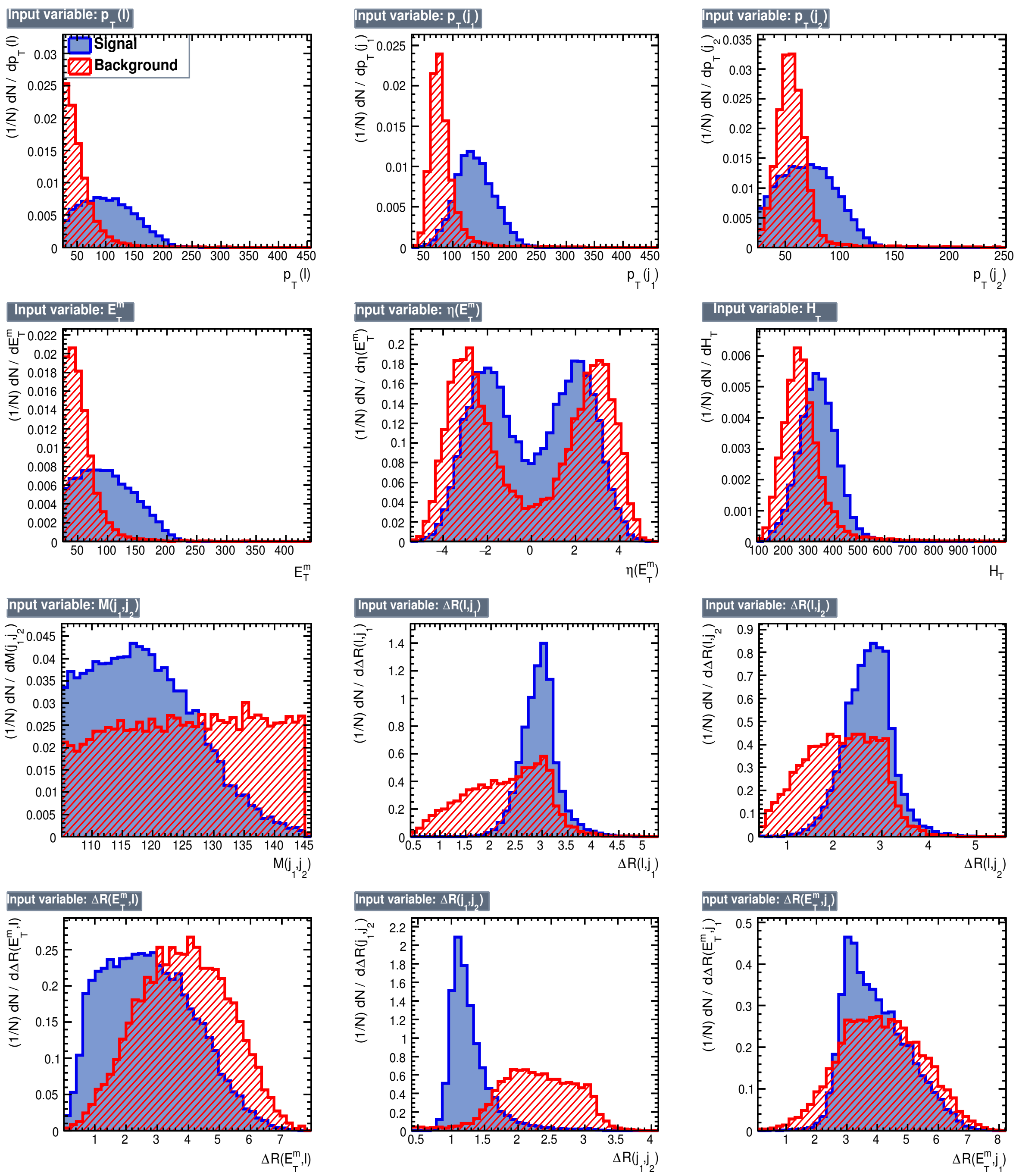

FIG. 3. The same as Fig. 2 but for $m_{H^\pm} = 500$ GeV.

are well-separated, and this can improve as we go to higher $m_{H^\pm}$ values. One then applies a BDT cut i.e. $\mathrm{BDT}_{res} > \mathcal{C}$, where $\mathcal{C} \in [-1, 1]$ on the signal and background samples. The corresponding cut efficiencies are shown as functions of $\mathcal{C}$ in Fig. 4b (Fig. 4d) for $m_{H^\pm} = 300$ GeV ($m_{H^\pm} = 500$ GeV). The optimal BDT cut (BDT_{opt}) is defined for which the significance $\mathcal{N}_S/\sqrt{\mathcal{N}_S + \mathcal{N}_B}$ is maximized (where $\mathcal{N}_S$ and $\mathcal{N}_B$ are the number of signal and background events, respectively, for a given luminosity that are survived after the BDT cut). We see in Fig. 4b that if we have, at least, 222 signal events (for $\mathcal{L} = 50$ fb^{-1}) before the BDT analysis, one can acheive a maximum 5σ significance for BDT$_{opt} \gtrsim 0.26$. After this cut, the number of signal events is reduced to 118 from 222 but the background events are drastically reduced to 436 from 33031. In Table IV, we show $\mathcal{N}_S$ and $\mathcal{N}_B$ along with $\mathcal{N}_S^{bc}$, the minimum number of signal events before the BDT cut that is required to achieve 5σ significance, for different $m_{H^\pm}$ values and for the two selection categories.

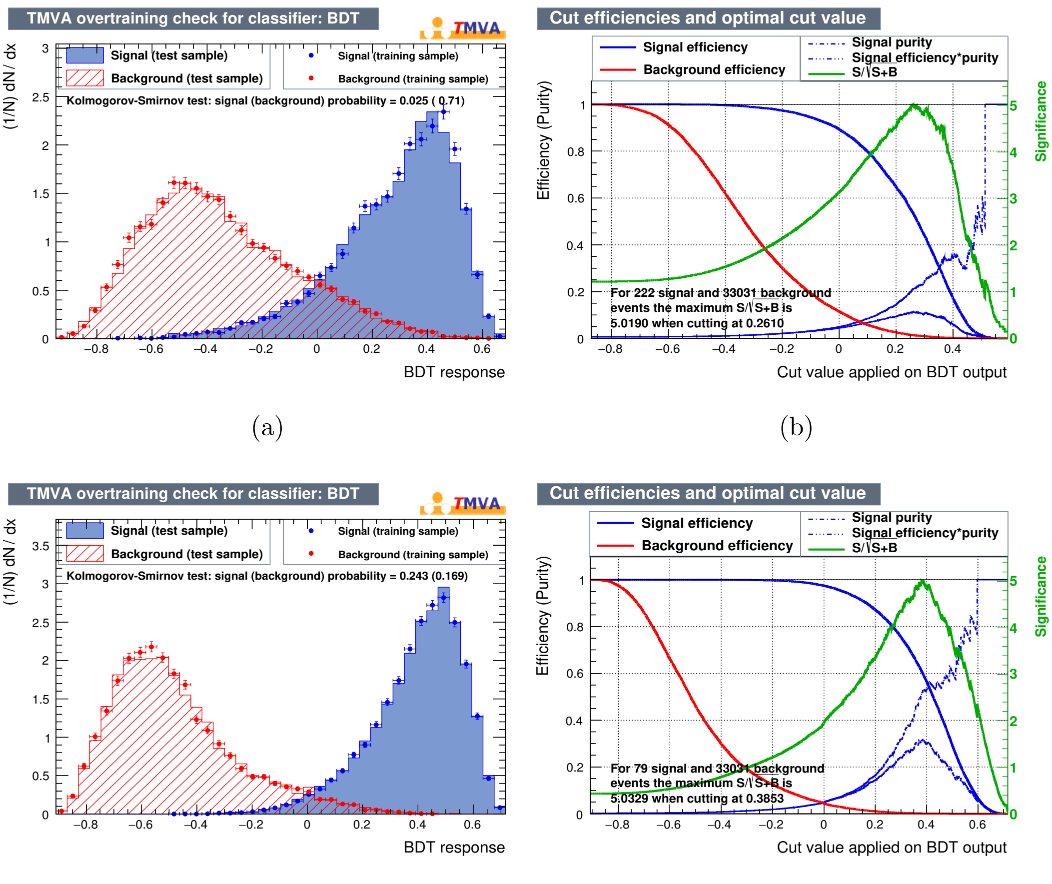

(a) (b)

(c) (d)

FIG. 4. (a) The BDT response for the signal and the background for $m_{H^\pm} = 300$ GeV at the LHC ($\sqrt{s} = 13$ TeV) for the 2b-tag category. (b) The corresponding signal and background cut efficiencies and significance as functions of the BDT cut. Discovery significance of 5σ is achieved for the optimal BDT cut, BDT$_{opt} \gtrsim 0.26$. Similar figures for $m_{H^\pm} = 500$ GeV are shown in (c) and (d) where a maximum 5σ significance is achieved for BDT$_{opt} \gtrsim 0.39$.

$m_{H^\pm}$	1b-tag category				2b-tag category			
(GeV)	$\mathcal{N}_S^{bc}$	BDT$_{opt}$	$\mathcal{N}_S$	$\mathcal{N}_B$	$\mathcal{N}_S^{bc}$	BDT$_{opt}$	$\mathcal{N}_S$	$\mathcal{N}_B$
250	1227	0.31	579	12796	260	0.23	151	758
300	983	0.42	341	4303	222	0.26	118	436
350	680	0.44	262	2485	176	0.29	99	295
500	229	0.48	49	47	79	0.39	47	41
800	149	0.43	55	66	60	0.44	37	17
$\mathcal{N}_{\rm SM}$	344173	-	-	-	33031	-	-	-

TABLE IV. The number of the SM background events ($\mathcal{N}_{\rm SM}$) for the 1b-tag category at the LHC ($\sqrt{s} = 13$ TeV) with $\mathcal{L} = 50$ fb^{-1} that enters in the MVA. The minimum number of signal events that can be discovered with 5σ significance using our MVA is denoted by $\mathcal{N}_S^{bc}$ (this is before the optimal BDT cut as shown in the third column). The signal and background events that survived after the optimal BDT cut are denoted by $\mathcal{N}_S$ and $\mathcal{N}_B$, respectively, and they lead to 5σ significance.

V. DISCOVERY REGIONS OF THE 3HDM PARAMETER SPACE

The question still remains: Does the model we proposed in section II predict signals leading to discovery using the presented analysis? In this section we find regions of the parameter space where that is the case, showing that if limits are set by the experimental collaborations the theory can be constrained using the current experimental data.

The first task is to match our model to the Lagrangian in Eqs. (31) and (32). For each parameter space point, we choose the lightest charged scalar for the analysis. Although we concentrated our search in the parameter space region with $v_{1,2} \ll v_3$, as to exploit the SM-like h_{125} state in that limit, we do not rely on the validity of the expansion in small ξ in this analysis. The couplings κ_{cs} and $\kappa_{Wh_{125}}$ are found in Eq. (23) after a numerical calculation of the spectrum and mixing matrices. To obtain the discovery reach of our parameter space, we translate $\mathcal{N}_S^{bc}$ in terms of the model parameters by using the following relation

$$\mathcal{N}_S^{bc} = \sigma(pp \to H^\pm \to W^\pm h_{125} \to \ell^\pm + \not{E}_T + b\bar{b}) \times \epsilon_S \times \mathcal{L}\,, \tag{37}$$

where σ is the cross section after showering and hadronization, ϵ_S is the signal cut efficiency and $\mathcal{L}$ is the integrated luminosity.

For the calculation of $\mathrm{BR}_{Wh_{125}}$, it is important to note that although in general $H^{\pm}$ can decay to $W^{\pm}h_{\mathrm{a,b,125}}$, we are interested only in the decay mode involving h_{125}, as in our model this is the state that couples the strongest to $b\bar{b}$ (see Eqs. (29) and (30)).

In addition, our model must be able to pass several consistency tests with the SM in order to be phenomenologically viable, such as reproducing the electroweak precision measurements. The original formulation [40] for beyond-the-SM contributions to the electroweak precision observables in terms of the S, T and U parameters assumes that the scale of new physics is $\gtrsim 1$ TeV. As our model allows for new exotic scalars to have masses around the electro-weak scale, we must employ the more general formalism introduced in Refs. [41, 42] with an extended set of oblique parameters S, T, U, V, W and X. These can then be used to calculate S', T' and U' for which the standard Z-pole constraints on S, T and U apply. To compute S', T' and U', we have applied the results in Ref. [43], in which S, T, U, V, W and X are computed for a general N-Higgs Doublet Model with the inclusion of arbitrary numbers of electrically charged and neutral $\mathrm{SU(2)_L}$ singlets. To summarize, when scanning the model parameter space for phenomenologically interesting regions, we look for points for which the following constraints are satisfied:

- There are no tachyonic scalar masses and the scalar potential is bounded from below (the corresponding constraints on the quartic couplings can be found in Ref. [8] taking into account that our λ_{ii} differ by a factor two from theirs).
- The tree-level scalar four-point amplitudes satisfy $|\mathcal{M}| < 4\pi$.
- The SM Higgs-like scalar has a mass no more than 5 GeV away from the observed 125 GeV value, and has a Yukawa coupling to the top quark satisfying $|y_{t\bar{t}h_{125}}| \in [0.9, 1.1]$.
- The exotic decays $Z \to h_{\mathrm{a,b}}A_{\mathrm{a,b}}$ are kinematically forbidden, as to not be in conflict with the precision measurements of the Z width.
- The lightest charged Higgs has a mass in the range $[m_{H^{\pm}}^{(\mathrm{min})}, 1000\,\mathrm{GeV}]$, with a different $m_{H^{\pm}}^{(\mathrm{min})}$ for each run (taking values 250, 300, 400 or 450 GeV).
- The computed values of S', T' and U' fall within the error bars on S, T and U as reported in Ref. [44].
- The value of $\kappa_{cs}^2 \times \mathrm{BR}_{Wh_{125}}$ is at least 0.5 above the 100 fb^{-1} discovery threshold for the 1b-tag category set by the MVA.

A. Scanning the parameter space

A random scan over the parameter space of the theory is both computationally expensive and not efficient. A good alternative, without the need for sophisticated statistical methods but still very powerful is the use of Genetic Algorithms (GA).
Following the guidelines set in Ref. [45], we wrote a GA in `Mathematica` for finding the parameter points in the discovery region, with a fitness function taking into account all the constraints listed above and including the so-called biodiversity punishment to explore the parameter space more thoroughly.
GAs start from a randomly generated initial population, with each full cycle resulting in a new generation of candidates. The fittest parameter points are selected for every generation and their parameters are modified (by crossover and/or mutations) leading to a new generation. The new candidate points are then used in the next iteration of the GA. The GA finishes when either a maximum number of generations or a satisfactory fitness level is reached. We decided to build the GA relying on mutations only as it usually performs comparably to GAs including a crossover but it is simpler to implement, and it was stopped once a number of valid parameter points was reached.

B. Results of the GA parameter scan

We performed five independent scans with different initial population sizes ranging from 50 to 1000, with varying mutation rates and different lower limits on $m_{H^\pm}$. We found 2116 parameter space points of the proposed model satisfying all the constraints within the discovery region of our analysis. In Figs. 5a and 5b, we show the 5σ discovery contours of $\kappa_{cs}^2 \times \mathrm{BR}_{Wh_{125}}$ corresponding to 1b- and 2b-tag categories, respectively, as functions of $m_{H^\pm}$ for $\mathcal{L} = 50, 100$ fb^{-1} at the LHC ($\sqrt{s} = 13$ TeV). Here, these functions are overlayed with the corresponding values for the parameter points found by the GA scanning procedure. We find that both selection categories are almost equally sensitive in probing the parameter space of our model. However, the 2b-tag category slightly more sensitive than the 1b-tag category since the background reduction is more proficient for the former. The irregularities in the charged Higgs mass dependence seen in Figs. 5a and 5b are due to a combination of points from scans with different lower limits on $m_{H^\pm}$.
As discussed before, since a W' can also produce a Wh_{125} resonance, we compare our

reach with the Wh_{125} resonance search data. In Fig. 5b, the shaded region is excluded from the ATLAS Wh_{125} resonance search data [35] in the $\ell + \not{E}_T + b\bar{b}$ channel. To obtain this, we translate the 95% confidence level (CL) upper limit (UL) on the cross section set by ATLAS in terms of our model parameters by using the following relation,

$$(\sigma \times \text{BR})_{UL} \times \epsilon_{W'} = \sigma(pp \to H^{\pm}) \times \text{BR}(H^{\pm} \to W^{\pm}h_{125}) \times \epsilon_{H^{\pm}} \tag{38}$$

where $\epsilon_{W'}$ and $\epsilon_{H^{\pm}}$ are the cut-efficiencies for the W' and $H^{\pm}$ respectively and they are different, in general. For simplicity, we assume $\epsilon_{W'} = \epsilon_{H^{\pm}}$ while obtaining the exclusion region on our model parameters. For instance, for $m_{H^{\pm}} = 800$ GeV, $\kappa^2 \times \text{BR}_{Wh_{125}} \gtrsim 2 \times 10^{-3}$ is excluded with 2σ CL using $\mathcal{L} \approx 36$ fb^{-1} data but $\kappa^2 \times \text{BR}_{Wh_{125}} \lesssim 2 \times 10^{-3}$ region can be discovered with 5σ significance if we go to a higher luminosity. The exclusion region starts from $m_{H^{\pm}} = 500$ GeV since the latest data used here are available from W' mass above 500 GeV.

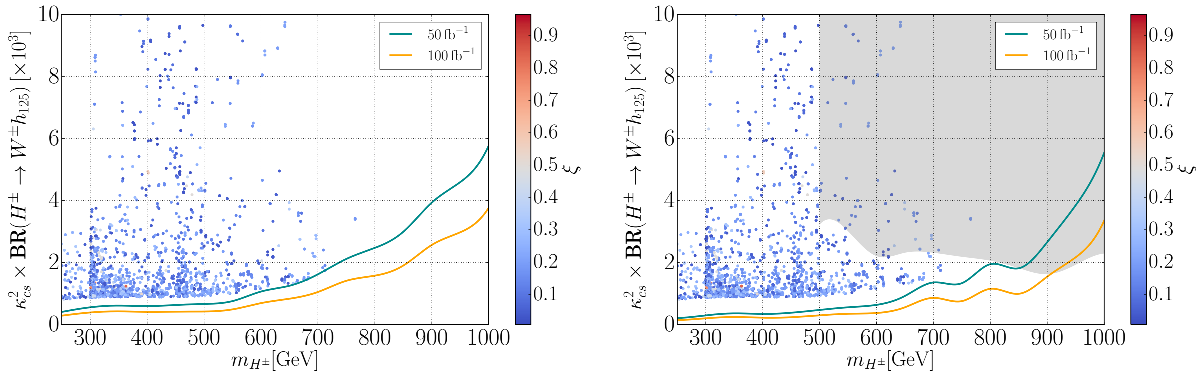

(a) (b)

FIG. 5. The 5σ discovery contours of $\kappa_{cs}^2 \times \text{BR}_{Wh_{125}}$ (scaled by 10^3) as functions of $m_{H^{\pm}}$ for $\mathcal{L} = 50, 100$ fb^{-1} at the LHC ($\sqrt{s} = 13$ TeV) for (a) 1b-tag category and (b) 2b-tag category. The dots represent the parameter points resulting form the GA scan with the corresponding values of ξ encoded in their color.

Although the lightest charged scalar (identified as $H^{\pm}$ for the analysis) does not primarily decay into Wh_{125}, it can still reach the discovery regions due to being mainly produced through $c\bar{s}$ fusion and having $\text{BR}(Wh_{125})$ comparable to the BR of the other decay channels. In Fig. 6a we show the $\text{BR}(H^{\pm} \to W^{\pm}h_{125})$ vs $\text{BR}(H^{+} \to c\bar{s})$ for the lightest charged scalar, where the dashed line represents the case when only the $W^{\pm}h_{125}$ and the $c\bar{s}$ ($\bar{c}s$) decay modes dominate. For the parameter points not close to this line, the remaining decay width is mostly due to the $H^{\pm}W^{\pm}h_{\rm a,b}$. For a few outlier points, the $H^{+} \to t\bar{b}$ mode is also relevant.

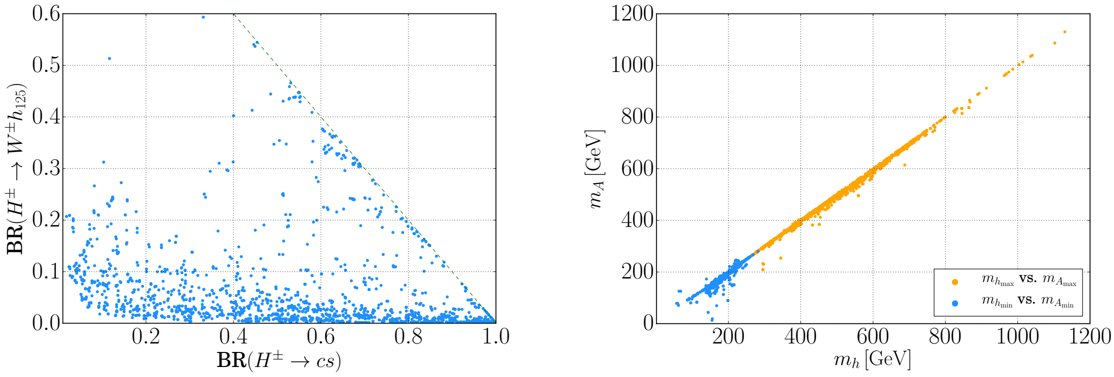

(a) (b)

FIG. 6. (a) BR($H^{+} \to W^{+}h_{125}$) vs. BR($H^{+} \to c\bar{s}$). The dashed line represents when BR($H^{+} \to W^{+}h_{125}$) + BR($H^{+} \to c\bar{s}$) = 1, i.e. when these two channels dominate the total decay width. For almost all points far away from this line, the lightest charged Higgs often decays to $W^{\pm}h_{\rm a,b}$. (b) Scalar vs. pseudo-scalar masses for the lightest (blue) and heaviest (orange) states. The alignment of these masses is consistent with the $\xi \ll 1$ expansion.

It is worth noting that although the GA did not rely on the validity of the $\xi \ll 1$ expansion, it often finds points with $\xi \ll 1$. Those points show a hierarchy in the VEVs of the scalar fields ($v_{1,2} \ll v_3$) and therefore a diminished hierarchy in the Yukawa couplings of the quark sector and all the features described in section II. That can also be seen in Figs. 5a–5b where we have indicated the specific values of ξ for the valid parameter points. We have checked the difference between the $\mathcal{O}(\xi)$ expressions for masses and the full numerical calculation, and find that for a vast majority of the valid parameter points the $\xi \ll 1$ expansion is reliable. However, there is still a small number of valid points incompatible with the ξ-expansion due to the smallness of one of m_{ij}^2. Such points would still be in the discovery region, although without the features that assume $\xi \ll 1$. As can be seen from Fig. 6b, the masses of the exotic scalars and pseudo-scalars tend to align as predicted by the $\xi \ll 1$ expansion (see Eq. (22)).

VI. SUMMARY AND CONCLUSIONS

In this article we have introduced a class of 3HDMs with a global $\mathrm{U(1)_X} \times \mathrm{U(1)_Z}$ family symmetry that is softly broken by bi-linear terms in the scalar potential. We have shown how to assign the X and Z charges of the fermions such that no tree-level FCNCs are present, while enforcing a Cabbibo-like structure of V_{CKM}. We described how a mixing with the third quark family can be induced from dim-6 operators, which would explain the smallness of the corresponding entries in V_{CKM}. Moreover, we showed that a hierarchy in the VEVs of the three Higgs doublets, $v_{1,2} \ll v_3$, leads to a heavy third quark family without the need for a strong hierarchy in the Yukawa couplings (contrary to what happens in the SM where e.g. $y_{\mathrm{up}}/y_{\mathrm{top}} \sim 10^{-5}$). The same hierarchy has been exploited to derive simple closed expressions for the scalar masses and mixing matrices by expansions in the small parameter $\xi \equiv \sqrt{v_1^2 + v_2^2}/v_3 \ll 1$.

A generic prediction of the model is that the new scalars $h_{\mathrm{a,b}}$, $A_{\mathrm{a,b}}$ and $H^{\pm}_{\mathrm{a,b}}$ are likely to couple strongly to the s and c quarks, yielding different signatures in colliders, at variance with standard searches focusing on the third quark family. As an example, we studied the collider phenomenology of the lightest charged Higgs when its mass is in the 250 – 1000 GeV range, under the assumption that the other charged Higgs is sufficiently heavy to be dropped out of the analysis. In that case, the lighter charged Higgs would be resonantly produced through a $c\bar{s}$ fusion, and, for certain regions of the parameter space, subsequently decay to Wh_{125}. All other decay channels are assumed to only contribute to its total width.

We particularly focused on one of the possible channels – the $c\bar{s} \to H^+ \to W^+ h_{125}$ channel, which has not been explored before in the context of heavier charged Higgs searches. This channel is specific to our class of 3HDMs and is particularly sensitive to the sub-TeV charged Higgs mass and small-ξ regions. We showed that this unconventional channel, when combined with the power of a multivariate analysis, leads to good signal-to-background ratios even for masses below 500 GeV and thus can be used to probe models with that particular feature at the LHC. We employed a model independent formulation so that our approach can be applied to any model which predicts a sufficiently large cross section for the $c\bar{s} \to H^+ \to W^+ h_{125}$ process to be observed at the future LHC runs. Our analysis can also be applied to improve sensitivity for W' searches especially for the sub-TeV masses.

We then showed how the analysis translates to the model we proposed by using a Genetic Algorithm to find parameter space points both within the discovery region and satisfying all the basic phenomenological constraints. Although the scan did not rely on $\xi \ll 1$, a vast majority of the points were consistent with that limit and thus showed all the features mentioned above and described in section II. This shows that this unconventional search strategy can effectively probe realistic theories with interesting features with the current LHC data, and thus we think it should be implemented by our experimental colleagues.

ACKNOWLEDGMENTS

The authors would like to thank Johan Rathsman for fruitful discussions. The work of T.M. is supported by the Swedish Research Council under contract 621-2011-5107 and 2015-04814 and the Carl Trygger Foundation under contract CTS-14:206. J. E. C.-M. was partially supported by Lund University. R.P. and J.W. were partially supported by the Swedish Research Council, contract numbers 621-2013-428 and 2016-05996. R.P. was also partially supported by CONICYT grant PIA ACT1406.

[1] G. C. Branco, P. M. Ferreira, L. Lavoura, M. N. Rebelo, Marc Sher, and Joao P. Silva. Theory and phenomenology of two-Higgs-doublet models. *Phys. Rept.*, 516:1–102, 2012.

[2] I. P. Ivanov and C. C. Nishi. Symmetry breaking patterns in 3HDM. *JHEP*, 01:021, 2015.

[3] A. G. Akeroyd, Stefano Moretti, Kei Yagyu, and Emine Yildirim. Light charged Higgs boson scenario in 3HDMs. In *Thunderstorms and Elementary Particle Acceleration: High-energy physics in atmosphere (TEPA-2016) Yerevan, Aragasotn, Armenia, October 3-7, 2016*, 2016.

[4] José Eliel Camargo-Molina, Roman Pasechnik, and Jonas Wessén. Charged scalars from $SU(3)^3$ theories. In *6th International Workshop on Prospects for Charged Higgs Discovery at Colliders (CHARGED 2016) Uppsala, Sweden, October 3-6, 2016*, 2017.

[5] Marco Merchand and Marc Sher. Three doublet lepton-specific model. *Phys. Rev.*, D95(5):055004, 2017.

[6] Stefano Moretti and Kei Yagyu. Constraints on Parameter Space from Perturbative Unitarity in Models with Three Scalar Doublets. *Phys. Rev.*, D91:055022, 2015.

[7] Dipankar Das and Ujjal Kumar Dey. Analysis of an extended scalar sector with S_3 symmetry. *Phys. Rev.*, D89(9):095025, 2014. [Erratum: Phys. Rev.D91,no.3,039905(2015)].

[8] Venus Keus, Stephen F. King, and Stefano Moretti. Three-Higgs-doublet models: symmetries, potentials and Higgs boson masses. *JHEP*, 01:052, 2014.

[9] The ATLAS collaboration. Search for charged Higgs bosons in the $H^{\pm} \to tb$ decay channel in pp collisions at $\sqrt{s} = 13$ TeV using the ATLAS detector. 2016.

[10] Vardan Khachatryan et al. Search for a charged Higgs boson in pp collisions at $\sqrt{s} = 8$ TeV. *JHEP*, 11:018, 2015.

[11] Howard Georgi and Marie Machacek. DOUBLY CHARGED HIGGS BOSONS. *Nucl. Phys.*, B262:463–477, 1985.

[12] Georges Aad et al. Search for a Charged Higgs Boson Produced in the Vector-Boson Fusion Mode with Decay $H^{\pm} \to W^{\pm}Z$ using pp Collisions at $\sqrt{s} = 8$TeV with the ATLAS Experiment. *Phys. Rev. Lett.*, 114(23):231801, 2015.

[13] Albert M Sirunyan et al. Search for charged Higgs bosons produced in vector boson fusion processes and decaying into a pair of W and Z bosons using proton-proton collisions at sqrt(s) = 13 TeV. 2017.

[14] Georges Aad et al. Search for charged Higgs bosons decaying via $H^{\pm} \to \tau^{\pm}\nu$ in fully hadronic final states using pp collision data at $\sqrt{s} = 8$ TeV with the ATLAS detector. *JHEP*, 03:088, 2015.

[15] Georges Aad et al. Search for a light charged Higgs boson in the decay channel $H^{+} \to c\bar{s}$ in $t\bar{t}$ events using pp collisions at $\sqrt{s} = 7$ TeV with the ATLAS detector. *Eur. Phys. J.*, C73(6):2465, 2013.

[16] Vardan Khachatryan et al. Search for a light charged Higgs boson decaying to $\mathrm{c\bar{s}}$ in pp collisions at $\sqrt{s} = 8$ TeV. *JHEP*, 12:178, 2015.

[17] CMS Collaboration. Search for Charged Higgs boson to $\mathrm{c\bar{b}}$ in lepton+jets channel using top quark pair events. 2016.

[18] J. Abdallah et al. Search for charged Higgs bosons at LEP in general two Higgs doublet models. *Eur. Phys. J.*, C34:399–418, 2004.

[19] G. Abbiendi et al. Search for Charged Higgs Bosons in e^+e^- Collisions at $\sqrt{s} = 189 - 209$ GeV. *Eur. Phys. J.*, C72:2076, 2012.

[20] Stefano Moretti. The $W^\pm$ h decay channel as a probe of charged Higgs boson production at the large hadron collider. *Phys. Lett.*, B481:49–56, 2000.

[21] Rikard Enberg, William Klemm, Stefano Moretti, Shoaib Munir, and Glenn Wouda. Charged Higgs boson in the $W^\pm$ Higgs channel at the Large Hadron Collider. *Nucl. Phys.*, B893:420–442, 2015.

[22] Stefano Moretti, Rui Santos, and Pankaj Sharma. Optimising Charged Higgs Boson Searches at the Large Hadron Collider Across $b\bar{b}W^\pm$ Final States. *Phys. Lett.*, B760:697–705, 2016.

[23] Stefan Dittmaier, Gudrun Hiller, Tilman Plehn, and Michael Spannowsky. Charged-Higgs Collider Signals with or without Flavor. *Phys. Rev.*, D77:115001, 2008.

[24] C.D. Froggatt and H.B. Nielsen. Hierarchy of quark masses, cabibbo angles and cp violation. *Nuclear Physics B*, 147(3):277 – 298, 1979.

[25] Adam Alloul, Neil D. Christensen, Cline Degrande, Claude Duhr, and Benjamin Fuks. FeynRules 2.0 - A complete toolbox for tree-level phenomenology. *Comput. Phys. Commun.*, 185:2250–2300, 2014.

[26] Celine Degrande, Claude Duhr, Benjamin Fuks, David Grellscheid, Olivier Mattelaer, and Thomas Reiter. UFO - The Universal FeynRules Output. *Comput. Phys. Commun.*, 183:1201–1214, 2012.

[27] J. Alwall, R. Frederix, S. Frixione, V. Hirschi, F. Maltoni, O. Mattelaer, H. S. Shao, T. Stelzer, P. Torrielli, and M. Zaro. The automated computation of tree-level and next-to-leading order differential cross sections, and their matching to parton shower simulations. *JHEP*, 07:079, 2014.

[28] Richard D. Ball et al. Parton distributions with LHC data. *Nucl. Phys.*, B867:244–289, 2013.

[29] Torbjorn Sjostrand, Stephen Mrenna, and Peter Z. Skands. PYTHIA 6.4 Physics and Manual. *JHEP*, 05:026, 2006.

[30] J. de Favereau, C. Delaere, P. Demin, A. Giammanco, V. Lematre, A. Mertens, and M. Selvaggi. DELPHES 3, A modular framework for fast simulation of a generic collider experiment. *JHEP*, 02:057, 2014.

[31] Matteo Cacciari, Gavin P. Salam, and Gregory Soyez. FastJet User Manual. *Eur. Phys. J.*, C72:1896, 2012.

[32] Matteo Cacciari, Gavin P. Salam, and Gregory Soyez. The Anti-k(t) jet clustering algorithm. *JHEP*, 04:063, 2008.

[33] Andreas Hocker et al. TMVA - Toolkit for Multivariate Data Analysis. *PoS*, ACAT:040, 2007.

[34] Partha Konar, Kyoungchul Kong, and Konstantin T. Matchev. $\sqrt{\hat{s}}_{min}$: A Global inclusive variable for determining the mass scale of new physics in events with missing energy at hadron colliders. *JHEP*, 03:085, 2009.

[35] The ATLAS collaboration. Search for heavy resonances decaying to a W or Z boson and a Higgs boson in final states with leptons and b-jets in 36.1 fb^{-1} of pp collision data at $\sqrt{s} = 13$ TeV with the ATLAS detector. 2017.

[36] Albert M Sirunyan et al. Combination of searches for heavy resonances decaying to WW, WZ, ZZ, WH, and ZH boson pairs in proton-proton collisions at sqrt(s) = 8 and 13 TeV. 2017.

[37] Jinmian Li, Riley Patrick, Pankaj Sharma, and Anthony G. Williams. Boosting the charged Higgs search prospects using jet substructure at the LHC. *JHEP*, 11:164, 2016.

[38] Riley Patrick, Pankaj Sharma, and Anthony G. Williams. Exploring a heavy charged Higgs using jet substructure in a fully hadronic channel. *Nucl. Phys.*, B917:19–30, 2017.

[39] Pushpalatha C. Bhat. Multivariate Analysis Methods in Particle Physics. *Ann. Rev. Nucl. Part. Sci.*, 61:281–309, 2011.

[40] Michael E. Peskin and Tatsu Takeuchi. Estimation of oblique electroweak corrections. *Phys. Rev. D*, 46:381–409, Jul 1992.

[41] Ivan Maksymyk, C. P. Burgess, and David London. Beyond s, t, and u. *Phys. Rev. D*, 50:529–535, Jul 1994.

[42] C.P. Burgess, Stephen Godfrey, Heinz Knig, David London, and Ivan Maksymyk. A global fit to extended oblique parameters. *Physics Letters B*, 326(3):276 – 281, 1994.

[43] W. Grimus, L. Lavoura, O.M. Ogreid, and P. Osland. The oblique parameters in multi-higgs-doublet models. *Nuclear Physics B*, 801(1):81 – 96, 2008.

[44] C. Patrignani et al. Review of Particle Physics. *Chin. Phys.*, C40(10):100001, 2016.

[45] José Eliel Camargo-Molina and Jonas Wessén. (in preparation).